JACC: CARDIOVASCULAR INTERVENTIONS
VOL. 10, NO. 8, 2017

ISSN 1936-8798/$36.00
PUBLISHED BY ELSEVIER
http://dx.doi.org/10.1016/j.jcin.2016.12.024

Effect of Coronary Anatomy and Hydrostatic Pressure on Intracoronary Indices of Stenosis Severity

Tobias Härle, MD,[a] Mareike Luz, MD,[a] Sven Meyer, MD, PhD,[a] Kay Kronberg, MD,[a] Britta Nickau, MD,[b] Javier Escaned, MD, PhD,[c] Justin Davies, MD, PhD,[d] Albrecht Elsässer, MD[a]

ABSTRACT

OBJECTIVES The authors sought to analyze height differences within the coronary artery tree in patients in a supine position and to quantify the impact of hydrostatic pressure on intracoronary pressure measurements in vitro.

BACKGROUND Although pressure equalization of the pressure sensor and the systemic pressure at the catheter tip is mandatory in intracoronary pressure measurements, subsequent measurements may be influenced by hydrostatic pressure related to the coronary anatomy in the supine position. Outlining and quantifying this phenomenon is important to interpret routine and pullback pressure measurements within the coronary tree.

METHODS Coronary anatomy was analyzed in computed tomography angiographies of 70 patients to calculate height differences between the catheter tip and different coronary segments in the supine position. Using a dynamic pressure simulator, the effect of the expected hydrostatic pressure resulting from such height differences on indices stenosis severity was assessed.

RESULTS In all patients, the left anterior and right posterior descending arteries are the highest points of the coronary tree with a mean height difference of -4.9 ± 1.6 cm and -3.8 ± 1.0 cm; whereas the circumflex artery and right posterolateral branches are the lowest points, with mean height differences of 3.9 ± 0.9 cm and 2.6 ± 1.6 cm compared with the according ostium. In vitro measurements demonstrated a correlation of the absolute pressure differences with height differences ($r = 0.993$; $p < 0.0001$) and the slope was 0.77 mm Hg/cm. The Pd/Pa ratio and instantaneous wave-free ratio correlated also with the height difference (fractional flow reserve $r = 0.98$; $p < 0.0001$; instantaneous wave-free ratio $r = 0.97$; $p < 0.0001$), but both were influenced by the systemic pressure level.

CONCLUSIONS Hydrostatic pressure variations resulting from normal coronary anatomy in a supine position influence intracoronary pressure measurements and may affect their interpretation during stenosis severity assessment.
(J Am Coll Cardiol Intv 2017;10:764–73) © 2017 by the American College of Cardiology Foundation.

Functional assessment of coronary stenoses using intracoronary pressure guidewires constitutes a simple and clinically important diagnostic tool in the catheterization laboratory. In practice, fractional flow reserve (FFR) is calculated as the ratio of the distal trans-stenotic pressure to the proximal coronary or aortic pressure during pharmacologically induced (usually adenosine-induced) hyperemia, assuming that the effect of boundary conditions such as central venous pressure is negligible (1). The instantaneous wave-free ratio (iFR) is a new adenosine-independent index of coronary stenosis

From the [a]Department of Cardiology, Klinikum Oldenburg, European Medical School Oldenburg-Groningen, Carl von Ossietzky University Oldenburg, Germany; [b]Department of Diagnostic and Interventional Radiology, Klinikum Oldenburg, European Medical School Oldenburg-Groningen, Carl von Ossietzky University Oldenburg, Germany; [c]Cardiovascular Institute, Hospital Clinico San Carlos, Madrid, Spain; and the [d]International Centre for Circulatory Health, National Heart and Lung Institute, Imperial College London, London, United Kingdom. The technical equipment for the dynamic pressure simulator was a loan from Volcano Corporation. Dr. Escaned has served as a consultant and a speaker at educational events for Philips Volcano and Boston Scientific. Dr. Davies is a consultant for Volcano Corporation; and holds licensed patents pertaining to the iFR technology. All other authors have reported that they have no relationships relevant to the contents of this paper to disclose.

Manuscript received October 11, 2016; revised manuscript received November 28, 2016, accepted December 16, 2016.

severity. For iFR calculation, the aforesaid pressures are measured and indexed during a specific diastolic wave-free period, when coronary resistance is most stable and minimized over the cardiac cycle (2).

This simple approach facilitates physiological assessment of coronary stenosis severity in the catheterization laboratory. However, it is potentially fraught by the boundary conditions and assumptions of the model. Thus, although stenosis location should, from a theoretical perspective, not influence FFR or iFR measurements, significant differences of both iFR and FFR values between anterior and posterior coronary territories have been observed in clinical practice (3,4), with higher values of both indices in the circumflex (CX), obtuse marginal, and right coronary arteries (RCA), when compared with the left anterior descending coronary artery (LAD) and its diagonal branches. This difference was independent of the effects of potential clinical and anatomic confounders (4).

We hypothesized that variations in hydrostatic pressure, related to coronary anatomy, might be the cause of these findings. This might be important, not only for the interpretation of conventional FFR or iFR measurements, but also for intracoronary pressure mapping, an increasingly used application of both indices, and for measurements of microcirculatory resistance.

In the study presented, we sought to analyze and quantify the impact of hydrostatic pressure on the results of intracoronary pressure measurements using an in vitro model. Furthermore, we aimed to quantify the height differences between the distal coronary vessels and the corresponding coronary ostia in real patients in a supine position in order to quantify a theoretical impact of hydrostatic pressure in vivo.

METHODS

STUDY POPULATION. From May 2015 to June 2016 a total of 190 elective coronary computed tomography angiographies (CTAs) were performed in our hospital. Inclusion criteria for this analysis was any elective coronary CTA with capture of the complete heart as well as the computed tomography (CT) table. Patients with incomplete opacification of the coronary vessels (n = 2), extensive artefacts (n = 1), and coronary anomalies (n = 2) were excluded from analysis. Overall, a number of 70 CTA was identified as appropriate for the intended analysis (Figure 1).

ANALYSIS OF CORONARY ARTERY HEIGHT DIFFERENCES. Coronary CTA was performed according to common standards using a CT scanner with 64 detector rows. Beta-blockers were administered intravenously if necessary, targeting a heart rate below 90 beats/min.

ABBREVIATIONS AND ACRONYMS

BMI = body mass index
CT = computed tomography
CTA = computed tomography angiography
CX = circumflex artery
DPS = dynamic pressure simulator
ECG = electrocardiogram
FFR = fractional flow reserve
iFR = instantaneous wave-free ratio
LAD = left anterior descending artery
LV = left ventricular
LVEF = left ventricular ejection fraction
Pa = mean systemic pressure
Pd = mean distal pressure
RCA = right coronary artery
RPD = right descending posterior artery
RPL = right posterolateral artery

FIGURE 1 Flow Chart of Patient Selection

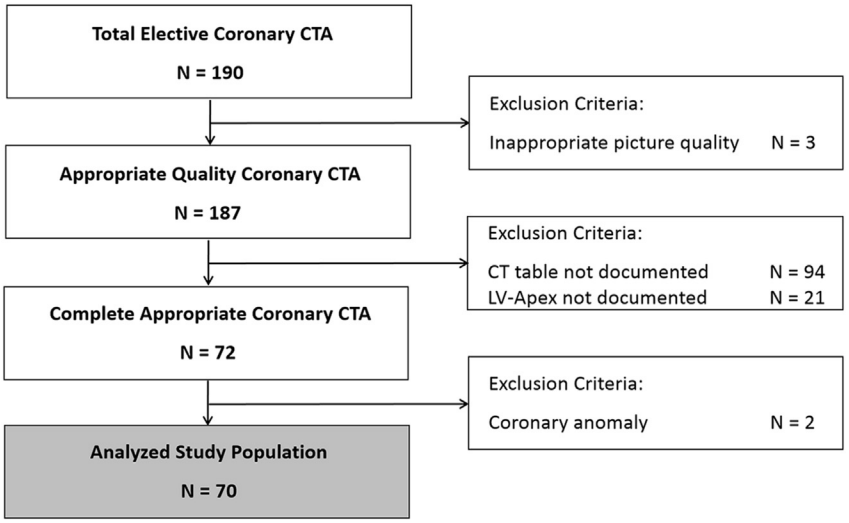

CT = computed tomography; CTA = computed tomography angiography; LV = left ventricular.

FIGURE 2 Dynamic Pressure Simulator for Pressure Measurements

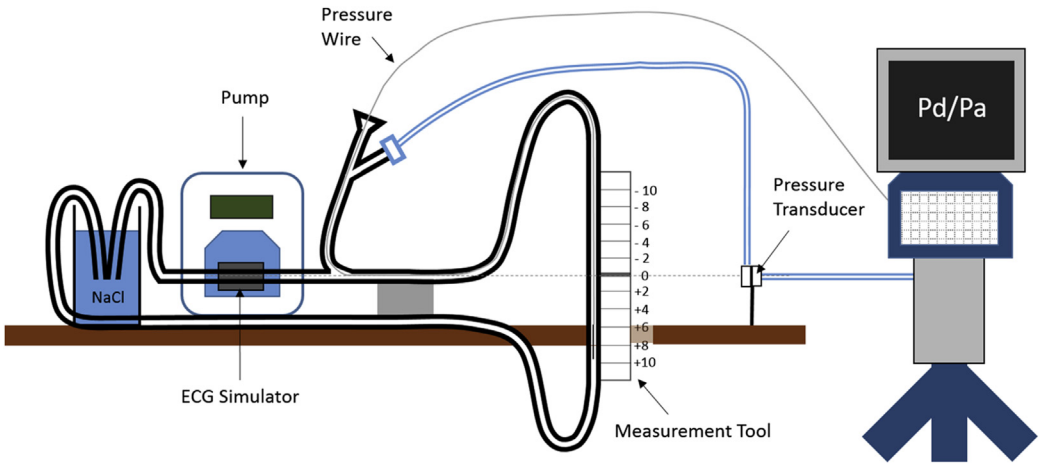

ECG = electrocardiogram; NaCl = sodium chloride solution; Pa = mean systemic pressure; Pd = mean distal pressure.

Scanning was performed with a slice thickness of 0.75 mm.

The course of the main branches of the left coronary artery (LCA) and RCA was mapped individually, that is, the LAD, the CX with its marginal branches, the right posterior descending coronary artery (RPD), and the right posterolateral coronary artery (RPL). For each of these vessels, the highest (maximum) and lowest (minimum) points of its course were identified, and its height was measured. The reference point for height measurements was the upper rim of the CT table, and the vertical distance to the center of the coronary artery at each measurement point was documented. Differences in the measured coronary artery height were calculated. As appropriate, negative algebraic signs reflect a higher anatomic point of measurement when compared with another point.

TABLE 1 Patient Characteristics

	All Patients	Female	Male	p Value
Patients, n	70 (100)	41 (58.6)	29 (41.4)	
Age, yrs	81 (76-85)	83 (80-87)	77 (69-82)	0.003
Height, cm	168 (160-172)	162 (157-168)	172 (168-178)	<0.001
Weight, kg	75 (63-81)	67.5 (58.5-75.5)	80 (76-90)	<0.001
BMI, kg/m^2	26.0 (23.8-28.1)	25.3 (22.5-27.9)	26.3 (24.8-29.4)	0.10
Arterial hypertension	61 (94)	38 (93)	23 (92)	0.62
Diabetes	15 (23)	9 (22)	6 (24)	0.89
Smoking	6 (9)	3 (8)	3 (12)	0.54
Dyslipidemia	25 (41)	13 (35)	12 (50)	0.25
LVEF, %	60 (55-65)	60 (60-65)	60 (47.5-62.5)	0.25
Aortic stenosis	59 (84)	38 (93)	21 (72)	0.02

Values are n (%) or median (interquartile range).
BMI = body mass index; LVEF = left ventricular ejection fraction.

DYNAMIC PRESSURE SIMULATOR. In vitro measurements were performed using a dynamic pressure simulator (DPS). The DPS utilizes a Masterflex Peristaltic Pump with a L/S computer-compatible digital drive (WU-07551-20, Cole-Parmer, Vernon Hills, Illinois) and a Masterflex L/S Pumphead (EW-07516-10, Cole-Parmer), a custom-made ECG simulator (Volcano Corporation, San Diego, California), various diameters of tubing (Masterflex L/S, Cole-Parmer; Tygon, McMaster-Carr, Chicago, Illinois), and standard pressure transducers (CODAN pvb Critical Care, Forstinning, Germany) to generate a dynamically changing pressure and flow environment (Figure 2). The ECG simulator was used to mimic an ECG signal by synchronizing a pulse wave to the peristaltic pump. It was connected to a S5 Imaging system (Volcano Corporation), which received systemic pressure (Pa) from the pressure transducer attached to the circuit of the DPS system. The middle part of the tubing was clamped into a custom-made tool for height variation and measurement (Figure 2). The DPS circuit was completely filled, bubble-free, with 0.9% saline at 22°C.

IN VITRO PRESSURE MEASUREMENTS. A 0.014-inch pressure sensor-tipped wire (PrimeWire Prestige, Volcano Corporation) was connected to the S5 Imaging system and inserted into the in vitro circuit

FIGURE 3 Normal Coronary CT Angiogram in Patients in a Supine Position

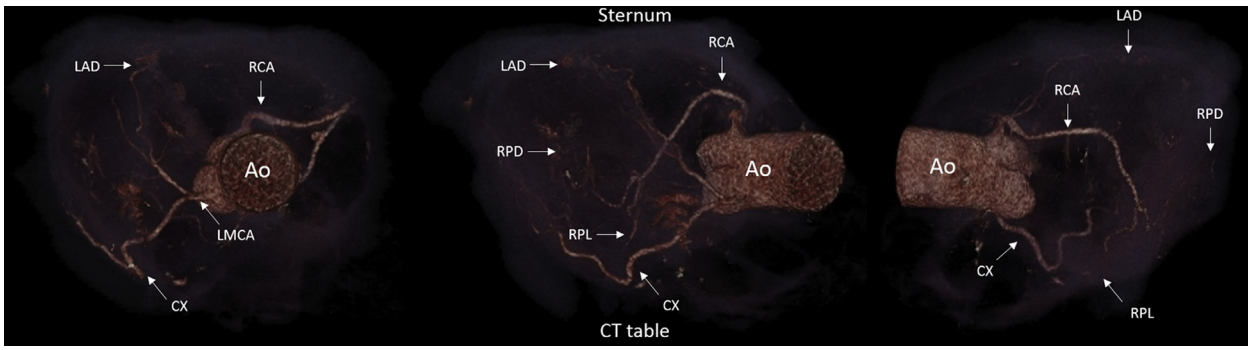

Three different views illustrate the course of the individual coronary arteries in patients in a supine position. Ao = aorta; CT = computed tomography; CX = circumflex coronary artery; LAD = left anterior descending coronary artery; LMCA = left main coronary artery; RCA = right coronary artery; RPD = right descending posterior coronary artery; RPL = right posterolateral coronary artery.

of the DPS via a standard Y-connector with a hemostasis valve. Pressure equalization was performed at the level of the pressure transducer, which was identical to the zero level of the measurement tool. Afterward, the wire was advanced into the measurement tool for pressure recordings. We performed repetitive intracoronary pressure measurements with stepwise variation of the height level of the guidewire pressure sensor in steps of 2 cm with a range of 10 cm to both directions from the zero level.

On every step, systemic (Pa) and distal (Pd) pressure as well as the Pd/Pa ratio were recorded using the FFR mode, and iFR was calculated automatically using the S5 Imaging system. This measurement series was repeated with different mean systemic pressures and heart rates, and all measurement series were performed twice. At the end of each measurement series, the pressure sensor was retracted to the zero level to preclude pressure drift of the wire. In the case of any pressure drift ≥0.01, the corresponding measurement series was discarded and repeated.

STATISTICAL ANALYSES. Continuous variables are presented as mean ± SD or median and interquartile range as appropriate, and categorical variables are presented as numbers and percentages. Data were compared using the Student *t* test or Mann-Whitney *U* test as appropriate.

Linear regression was used to assess effects of variables on the maximal height difference of the highest to the lowest point of the coronary artery tree. We performed univariate analyses, considering explanatory variables, such as age, sex, body height, body weight, body mass index (BMI), body surface area, hypertension, and left ventricular ejection fraction (LVEF) separately as covariates, and we also evaluated the independent effects of these variables in an explanatory multivariate model. Additionally, we used the Furnival-Wilson leaps-and-bounds algorithm and performed all-subsets variable selection to construct a parsimonious predictive linear

FIGURE 4 Coronary Artery Heights in a Supine Position of the Patient

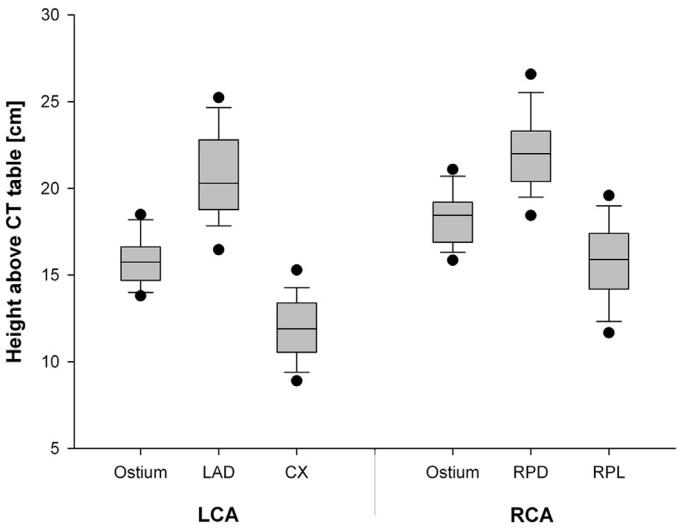

Box plots of the coronary artery heights above the CT table for both coronary ostia, the highest points of LAD and RPD and the lowest points of CX und RPL. **Boxes** represent the median and the 25th and 75th percentiles, **error bars** represent the 10th and 90th percentiles, and **dots** represent the 5th and 95th percentiles. LCA = left coronary artery; other abbreviations as in Figure 3.

TABLE 2 Height Differences of Coronary Arteries in a Supine Patient Position

Height Differences	All Patients	Female	Male	p Value
LCA ost − RCA ost, cm	2.5 ± 0.6 2.5 (2.1 to 2.9)	2.4 ± 0.5 2.3 (2.1 to 2.8)	2.7 ± 0.5 2.8 (2.4 to 3.2)	0.01
LCA ost − LAD max, cm	−4.9 ± 1.6 −4.6 (−6.1 to −3.8)	−4.3 ± 1.4 −4.0 (−4.8 to −3.5)	−5.8 ± 1.3 −6.0 (−6.4 to −4.6)	<0.001
LCA ost − CX min, cm	3.9 ± 0.9 3.9 (3.3 to 4.6)	4.0 ± 0.9 4.0 (3.3 to 4.6)	3.7 ± 0.9 3.7 (3.3 to 4.2)	0.21
CX min − LAD max	−8.8 ± 1.3 −8.8 (−9.6 to −8.0)	−8.3 ± 1.1 −8.2 (−9.0 to −7.6)	−9.5 ± 1.2 −9.6 (−10.1 to −9.0)	<0.001
RCA ost − RPD max, cm	−3.8 ± 1.0 −3.8 (−4.5 to −3.0)	−3.3 ± 0.7 −3.3 (−3.8 to −2.8)	−4.6 ± 0.8 −4.3 (−5.1 to −4.2)	<0.001
RCA ost − RPL min, cm	2.6 ± 1.6 2.7 (1.3 to 3.6)	2.6 ± 1.7 2.6 (1.3 to 3.6)	2.6 ± 1.5 2.7 (1.3 to 3.1)	0.99
RPL min − RPD max, cm	−6.5 ± 1.8 −6.6 (−7.6 to −5.5)	−5.9 ± 1.7 −5.9 (−6.9 to −4.8)	−7.2 ± 1.8 −7.4 (−8.3 to −6.0)	0.004
All max − All min, cm	10.4 ± 1.2 10.3 (9.5 to 11.0)	9.8 ± 0.9 9.8 (9.2 to 10.3)	11.2 ± 1.2 11.1 (10.4 to 11.5)	<0.001

Values are mean ± SD and median (interquartile range).

CX = circumflex artery; LAD = left anterior descending artery; LCA = left coronary artery; max = highest point of the vessel; min = lowest point of the vessel; ost = ostium; RCA = right coronary artery; RPD = right posterior descending artery; RPL = right posterolateral artery.

regression model on the basis of the Bayesian information criterion to identify the best fitting regression model.

RESULTS

STUDY POPULATION. Patient characteristics are summarized in Table 1. Most coronary CTA was performed in patients with planned transcutaneous aortic valve implantation due to severe aortic stenosis (84%). The median patient age was 81 years, with 41 female patients (58.6%). The latter were significantly older and more frequently had aortic stenosis when compared with male patients, but cardiovascular risk factors including BMI and LVEF were not different between the groups (Table 1).

ANALYSIS OF CORONARY ARTERY HEIGHT DIFFERENCES. Despite individual variations of coronary anatomy and cardiac topography, evaluation of the coronary anatomy with a focus on height differences in patients in a supine position revealed different, characteristic courses of each coronary artery (Figure 3). The ostium of the LCA was lower than the ostium of the right coronary artery (RCA) in all patients (100%), and the mean difference was 2.5 ± 0.6 cm ($p < 0.0001$). After a slight downward course up to the left main bifurcation, the LAD took an upward course in all patients (100%) with a mean height difference between the highest point of the LAD, which usually was at the left ventricular (LV) apex, and the LCA ostium of 4.9 ± 1.6 cm ($p < 0.0001$). Although the LCA ostium was nearly the lowest point in the course of the LAD, it was the highest point in the course of the CX in all patients (100%). The CX took a downward course in all patients, with mean height differences between the lowest point of the CX and the LCA ostium of 3.9 ± 0.9 cm ($p < 0.0001$) and the highest point of the LAD of 8.8 ± 1.3 cm ($p < 0.0001$).

The course of the RCA was usually upwards in the proximal one-third with a subsequent downward course up to the crux cordis. From there, the RPL trekked further downward and became the lowest point of the RCA in all patients (100%), with a mean height difference from the RCA ostium of 2.6 ± 1.6 cm ($p < 0.0001$). By contrast, the RPD took an upward course in the direction of the LV apex. The distal RPD was the highest point of the RCA in all patients (100%), with a mean height difference between the highest point and the ostium of the RCA of 3.8 ± 1.0 cm ($p < 0.0001$). The mean height difference between the highest point of the RPD and the lowest point of the RPL was 6.5 ± 1.8 cm ($p < 0.0001$) (Figure 4, Table 2).

SEX DIFFERENCES IN CORONARY HEIGHT DIFFERENCES. In general, the course of the coronary arteries was similar in female and male patients. The height differences of the LAD and RPD when compared with their coronary ostium was significantly lower in female patients (LAD 4.3 vs. 5.8 cm; $p < 0.001$; RPD

3.3 vs. 4.6 cm; $p < 0.001$), whereas there were no differences in the lowest point of the CX ($p = 0.21$) and the RPL of the RCA ($p = 0.99$) (Table 2).

DETERMINANTS OF HEIGHT DIFFERENCES. Univariate linear regression established that sex, body height, body weight, BMI, body surface area, hypertension, and LVEF have significant effects on the maximal height difference between the highest and the lowest point of the coronary artery tree if considered individually. Explanatory multivariate linear regression analysis showed that sex and LVEF independently affect the maximal height difference (Table 3). The all possible subsets variable selection approach resulted in a model of sex, LVEF, and BMI to best fit the data ($F[3,60] = 21.65$; $p = 0.0001$; 50% explained variability of the maximal height difference). Holding the other respective predictors in the model constant, women have a mean decrease in the maximal height difference of 1.22 cm compared with men; each percent increase in LVEF decreased the maximal height difference by 0.04 cm, and each unit increase of the BMI increased the maximal height difference by 0.08 cm.

IN VITRO PRESSURE MEASUREMENTS. Intracoronary pressure measurements were simulated in vitro using a DPS. Stepwise variation of the height of the distal pressure sensor resulted in significant differences of the measured distal pressure (Table 4). The absolute pressure difference of distal and systemic pressure was highly reproducible and independent of the systemic pressure level and the heart rate (Figure 5A). The absolute pressure difference correlated strongly with the height difference ($r = 0.993$; $p < 0.0001$) and the slope was 0.77 mm Hg/cm height difference (Figure 5B). FFR ratio and iFR also correlated strongly with the height difference (FFR $r = 0.98$; $p < 0.0001$; iFR $r = 0.97$; $p < 0.0001$), but both were influenced by the systemic pressure level, but not by the heart rate (Figures 5C and 5D).

TABLE 3 Determinants for the Maximal Height Difference

	Univariate		Multivariate	
	Coefficient (95% CI)	p Value	Coefficient (95% CI)	p Value
Age	0.02 (−0.02 to 0.06)	0.744	0.02 (−0.02 to 0.06)	0.340
Sex	−1.18 (−1.81 to −0.56)	<0.001	−1.18 (−1.81 to −0.56)	<0.001
Body height	−0.11 (−0.36 to 0.14)	0.001	−0.11 (−0.36 to 0.14)	0.373
Body weight	0.15 (−0.08 to 0.38)	<0.001	0.15 (−0.08 to 0.38)	0.191
Body mass index	−0.31 (−0.83 to 0.21)	0.005	−0.31 (−0.83 to 0.21)	0.243
Body surface area	−0.68 (−19.86 to 18.49)	<0.001	−0.68 (−19.86 to 18.49)	0.943
Hypertension	−0.78 (−1.84 to 0.29)	0.025	−0.78 (−1.84 to 0.29)	0.150
LVEF	−0.03 (−0.05 to −0.01)	0.001	−0.03 (−0.05 to −0.01)	0.016

CI = confidence interval; LVEF = left ventricular ejection fraction.

DISCUSSION

The main findings of the present study are as follows: 1) in our study population, the mean height difference of coronary segments interrogated with FFR was 10.4 ± 1.2 cm; 2) variations in hydrostatic pressure resulting from the location of the pressure wire sensor within that range of height values translates into significant differences in FFR and iFR, compared with the theoretical measurements; and 3) the effect of hydrostatic pressure on FFR and iFR values is inversely proportional to aortic pressure. These aspects are discussed in detail in the following paragraphs.

In intracoronary pressure measurements, pressure equalization of the distal pressure sensor with the systemic pressure at catheter tip is a methodically mandatory step. Subsequently, the distal pressure sensor should be positioned at the very distal part of the coronary artery for pressure measurement (5). Because there might be a height difference between the distal vessel and the catheter tip, an influence of hydrostatic pressure on the distally measured coronary pressure, which would lead to biased results of FFR and iFR calculation, would be reasonable. The results of our in vitro measurements confirm this hypothesis, and the extent of this influence approximates the theoretical expected impact of 0.74 mm Hg per cm on the basis of Pascal's law. According to the latter, the hydrostatic pressure (p[h]) is the product of mass density (ρ), gravity ($g = 9.81\ m/s^2$), and height difference (h): $(p[h] = \rho \cdot g \cdot h)$.

We found an impact of hydrostatic pressure on intracoronary pressure measurements of 0.77 mm Hg/cm height difference. Due to technical specifications of the DPS, measurements were performed with 0.9% saline at 22°C; such saline has a mass density of 1,004.6 kg/m^3 (6). Mass density values of blood depend on plasma protein concentration, hematocrit (7), and temperature (8). Under normal in vivo conditions, the mass density of blood approximates 1,050 kg/m^3 (9). Hence, a slightly higher impact of about 0.8 mm Hg/cm is expectable in vivo.

An important finding is that the modification caused by hydrostatic pressure on FFR and iFR values is inversely related to aortic pressure. In the case of FFR, this is relevant for the mode of adenosine administration used to induce hyperemia, because intravenous adenosine infusion may cause a major drop in aortic pressure, particularly in obese and diabetic patients (10). Both iFR and FFR measured during intracoronary injection of adenosine should be less sensitive to this source of error.

TABLE 4 Influence of Height Differences on Pressure Measurements in Vitro

		HR							
		60 Beats/Min				80 Beats/Min			
	Height, cm	Pd	Pd-Pa	Pd/Pa	iFR	Pd	Pd-Pa	Pd/Pa	iFR
Pa 80 mm Hg									
	Above								
	−10	72	−8	0.90	0.86	72	−8	0.90	0.88
	−8	74	−7	0.92	0.89	74	−6	0.93	0.91
	−6	76	−5	0.94	0.92	75	−5	0.94	0.93
	−4	77	−3	0.96	0.94	77	−3	0.96	0.95
	−2	79	−2	0.98	0.97	78	−2	0.98	0.97
	0	80	0	1.00	0.99	80	0	1.00	0.99
	Below								
	+2	82	2	1.03	1.01	82	2	1.03	1.02
	+4	83	3	1.04	1.03	83	3	1.04	1.03
	+6	85	5	1.06	1.06	85	5	1.06	1.06
	+8	86	6	1.08	1.08	86	6	1.08	1.08
	+10	88	8	1.10	1.10	88	8	1.10	1.10
Pa 100 mm Hg									
	Above								
	−10	92	−9	0.92	0.90	93	−7	0.93	0.89
	−8	94	−7	0.94	0.92	94	−6	0.94	0.91
	−6	95	−5	0.95	0.94	96	−4	0.96	0.93
	−4	97	−4	0.97	0.96	97	−3	0.97	0.95
	−2	99	−2	0.99	0.97	99	−1	0.99	0.96
	0	100	0	1.00	0.99	100	0	1.00	0.98
	Below								
	+2	102	2	1.02	1.01	102	2	1.02	1.00
	+4	103	3	1.03	1.03	104	4	1.04	1.02
	+6	104	4	1.04	1.05	105	5	1.05	1.03
	+8	106	6	1.06	1.06	106	6	1.06	1.05
	+10	107	7	1.07	1.09	108	8	1.08	1.07
Pa 120 mm Hg									
	Above								
	−10	113	−7	0.94	0.93	112	−8	0.93	0.91
	−8	115	−6	0.95	0.95	114	−6	0.95	0.93
	−6	116	−4	0.97	0.96	115	−5	0.96	0.94
	−4	118	−2	0.98	0.98	117	−3	0.98	0.95
	−2	119	−1	0.99	0.99	118	−2	0.98	0.97
	0	120	0	1.00	1.00	120	0	1.00	0.98
	Below								
	+2	123	3	1.02	1.02	122	2	1.02	1.00
	+4	124	4	1.03	1.04	123	3	1.03	1.01
	+6	125	5	1.04	1.05	124	4	1.03	1.02
	+8	127	7	1.05	1.07	125	5	1.04	1.03
	+10	128	8	1.07	1.08	127	7	1.06	1.05

HR = heart rate; iFR = instantaneous wave-free ratio; Pa = mean systemic pressure; Pd = mean distal pressure.

In the first part of our study, we sought to quantify the expectable impact of hydrostatic pressure on intracoronary pressure measurements in clinical practice. For this purpose, we evaluated the height differences within the coronary artery tree, in particular the height differences between distal coronary arteries and their coronary ostia in patients in a supine position, analyzing coronary CTA. Despite common variations in the coronary artery anatomy and cardiac topography, we were able to identify different, characteristic courses of each coronary artery. In patients in a supine position, the distal LAD and the distal RPD are the highest points of their corresponding coronary artery in all patients, with a significant mean height difference when compared with its coronary ostia of 4.9 cm and 3.8 cm, respectively. Assuming an impact of 0.8 mm Hg/cm in vivo, the distal coronary pressure (Pd) indexed for FFR and iFR calculation would be reduced by 3.9 mm Hg (LAD) and 3.0 mm Hg (RPD) due to hydrostatic pressure. Assuming a mean systemic pressure of 100 mm Hg, this would lead to FFR or iFR values of 0.96 and 0.97, respectively, in healthy vessels without coronary artery disease. On the other hand, the distal CX and the distal RPL are the lowest points of their corresponding coronary artery in all patients, with a significant mean height difference when compared with its coronary ostia of 3.9 cm and 2.6 cm, respectively. In these vessels, the impact of hydrostatic pressure would increase the Pd by 3.1 mm Hg (CX) and 2.1 mm Hg (RPL) leading to FFR or iFR values of 1.03 and 1.02, respectively. These data explain the previously published findings of FFR, and in particular iFR, values >1, as well as systematically higher FFR and iFR values, in posterior vessels when compared with anterior vessels (3,4). Because the hydrostatic pressure caused an absolute pressure difference in our study, its impact on both FFR and iFR would be more prominent, the lower the mean systemic pressure is. The clinical impact of variations in FFR and iFR is largely dictated by the characteristics of the study population, leading to more changes in stenosis severity classification when the median FFR or iFR value is close to the cutoff used to define stenosis severity in a dichotomous fashion (11).

The findings of our study provide an alternative explanation to the gradual loss of pressure observed in longitudinal pressure pullbacks by De Bruyne et al. (12) performed in both normal and diffusely narrowed coronary arteries. The variations in FFR recorded in angiographically normal vessels during a pressure guidewire pullback with intravenous adenosine infusion were 0.03 ± 0.02, and 0.11 ± 0.08 in vessels with diffuse narrowing, but without focal stenoses, and was interpreted in both cases as a result of the distribution of vascular resistance over the vessel, and not a result of the effect of hydrostatic pressure. Because longitudinal vessel mapping with FFR and iFR (13) is currently receiving great interest in clinical practice, further research is advisable on how to perform corrections for the deviations in the values of

FIGURE 5 Correlation of In Vitro Pressure Measurements and Height Differences

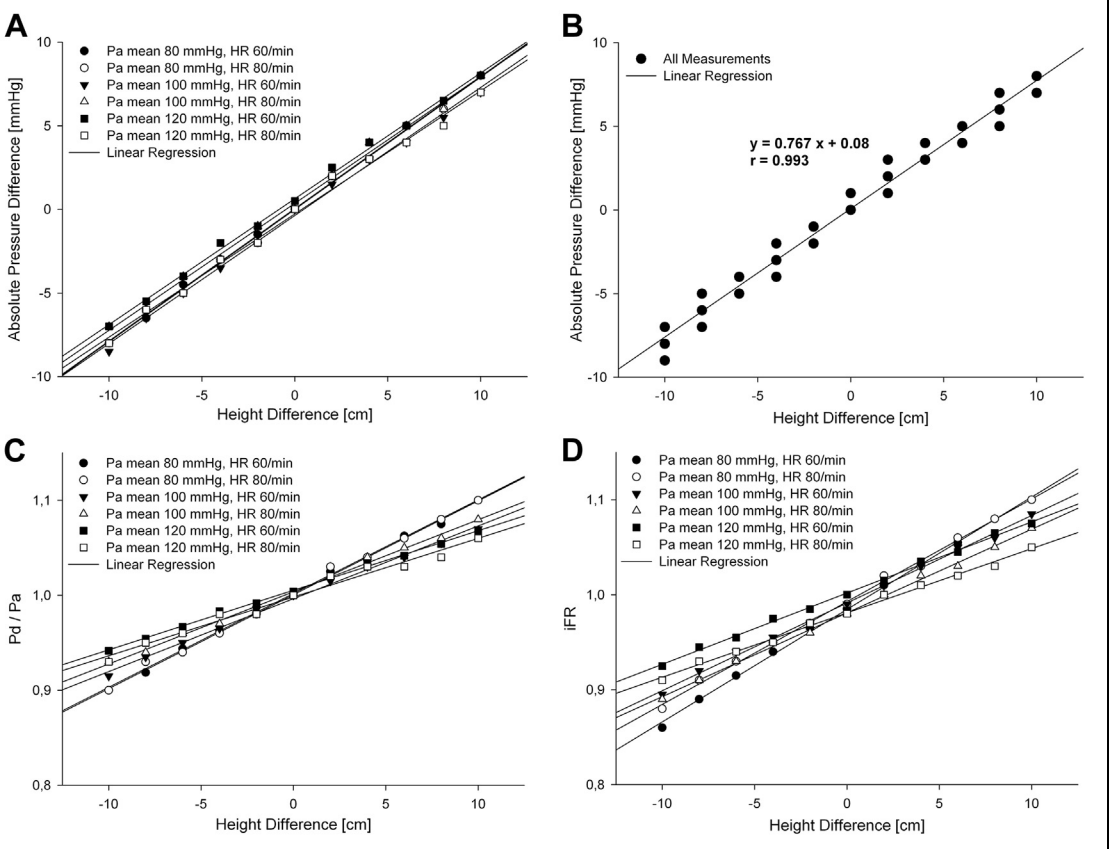

(A) The correlation between absolute pressure difference and height difference for different levels of mean systemic pressures and heart rates. **(B)** The correlation between absolute pressure difference and height difference combining all measurement series. **(C)** The correlation between the ratio of mean distal pressure and Pa mean and height difference for different levels of Pa mean and HR. **(D)** The correlation between the instantaneous wave-free ratio and height difference for different levels of Pa mean and HR. HR = heart rate; iFR = instantaneous wave-free ratio; other abbreviations as in Figure 2.

both indices attributable to variations in relative sensor height during vessel mapping.

However, it should be considered that in particular cases, the pressure sensor is positioned just 2 to 3 cm distal to the interrogated stenosis. Furthermore, the pressure sensor is located 3 cm proximal of the guidewire tip. This fact might be an argument for a less important impact of hydrostatic pressure in vivo. On the other hand, there are some aspects that might attenuate this argument. First, it seems likely that evaluation of coronary CTA did not identify the most distal parts of the coronary vessels in all cases, so the height differences in daily practice might be even higher. Second, the highest and lowest points of the coronary artery tree are not always the most distal points. In 2 recently published studies, the LAD was wrapped around the LV apex and supplying the apical inferior aspect of the heart in 55.6% and 76.3% of patients, respectively (14,15). Third, the course of coronary arteries is usually not strictly vertical, so the height difference between pressure sensor and guidewire tip is <3 cm in these cases. Fourth, coronary artery tortuosity is a common phenomenon (16,17), which might reduce the height distance of the pressure sensor and guidewire tip. Fifth, our reference population consisted predominantly of older women with a relatively low body height. Accordingly, more pronounced height differences are expectable in a common population undergoing elective coronary angiography for stable coronary artery disease, which usually consists predominantly of men. Altogether, it might be expected that

hydrostatic pressure has significant impact on intracoronary pressure measurements in some vessels, whereas it is negligible in others.

In daily clinical practice, our findings might be particularly important for intracoronary pressure measurements of main stem RCA stenosis. Most likely, positioning of the pressure guidewire in the RPD or RPL is an arbitrary decision in the majority of these cases. Because we found a mean height difference of 6.5 cm between these 2 vessels, different FFR and iFR values for stenoses of the RCA can be expected dependent on an anterior or posterior positioning of the guidewire. However, further clinical research is necessary to prove this theory in vivo.

Despite its impact on distal coronary artery pressure, hydrostatic pressure might influence intracoronary pressure measurements in vivo further by differences between anterior and posterior coronary venous pressures. According to the pivotal study, FFR is the relation of the difference between coronary pressure distal to a stenosis (Pd) and mean central venous pressure (Pv) and the difference between mean aortic pressure (Pa) and Pv [FFR = (Pd − Pv)/(Pa − Pv)] (18). For reasons of simplification, venous pressure was neglected in FFR calculation in the course (1,19). But, recently published data suggested that accounting for venous pressure lead to lower FFR values and reclassification of lesion severity (20). However, further investigations are necessary to prove this hypothesis.

With regard to clinical characteristics that might influence the maximal height difference, our explanatory multivariate linear regression analysis showed that sex and LVEF are independently associated with the maximal height difference. Both being a woman and having an increase in LVEF decreased the maximal height difference. Additionally, we found significantly less pronounced height differences in women for the LAD and the RPD. This phenomenon might be explained by well-established sex differences in LV size and remodeling in response to pressure overload, the underlying pathomechanism in aortic stenosis, which was the predominant indication for CTA in our reference population. Women with aortic stenosis have smaller left ventricles and less LV mass when compared with men (21,22). Furthermore, at comparable pressure overload levels, men exhibit a more eccentric form of LV hypertrophy with more frequent LV dilation (23). This might explain the less pronounced differences between anterior and posterior coronary vessels in women compared with men. Interestingly, age was not found to be associated with the maximal height difference. However, this might be referred to the overall high age of our study population.

Another aspect for which our findings may be relevant is the calculation of microcirculatory resistance. Both the thermodilution-based index of microcirculatory resistance (24) and the Doppler-based hyperemic microcirculatory resistance (25) index require the use of intracoronary pressure. Thus, the aforementioned modifications of the latter by hydrostatic pressure will likely lead to over- or underestimation of microcirculatory resistance. This is most likely the case of IMR: because intravenous infusion is mandatory for the calculation of this index, a more pronounced decrease in aortic pressure may contribute to magnifying the described effect.

STUDY LIMITATIONS. Measurements were performed using an in vitro model with silicone tubing, which might have different characteristics when compared with native human vessels. Therefore, transferability of our data on a physiological setting in vivo is necessary in order to confirm our findings. In particular, a possible influence of adenosine-induced hyperemia remains unclear to date. The majority of patients had aortic stenosis. Due to LV hypertrophy and a possible distortion of the aorta with a more horizontal heart, the height differences within the coronary tree might be different in a normal population. Nevertheless, our study proves a significant influence of hydrostatic pressure on the results of intracoronary pressure measurements.

CONCLUSIONS

Hydrostatic pressure variations resulting from normal coronary anatomy in a supine patient position influence intracoronary pressure measurements and may affect their interpretation during stenosis severity assessment.

ACKNOWLEDGMENTS The authors thank David Galliaerdt, Anton Ramos, and all the other project collaborators from Volcano Corporation for their support in establishing the dynamic pressure sensor.

ADDRESS FOR CORRESPONDENCE: Dr. Tobias Härle, Klinikum Oldenburg, Department of Cardiology, Rahel-Straus-Strasse 10, 26133 Oldenburg, Germany. E-mail: t.haerle@gmx.de.

PERSPECTIVES

WHAT IS KNOWN? For the first time to our knowledge, we provide evidence for an influence of hydrostatic pressure on intracoronary pressure measurements, and quantified height differences of the different coronary arteries in patients in a supine position.

WHAT IS NEW? The combination of both findings uncovers a systematic error that is of clinical relevance because it questions the accuracy of pressure measurements and in particular the use of 1 single cutoff value for all coronary vessels.

WHAT IS NEXT? If these findings can be confirmed in vivo, implementation of hydrostatic pressure into iFR and FFR calculation algorithms would be necessary.

REFERENCES

1. Pijls NH, Van Gelder B, Van der Voort P, et al. Fractional flow reserve: a useful index to evaluate the influence of an epicardial coronary stenosis on myocardial blood flow. Circulation 1995;92:3183–93.

2. Sen S, Escaned J, Malik IS, et al. Development and validation of a new adenosine-independent index of stenosis severity from coronary wave-intensity analysis: results of the ADVISE (ADenosine Vasodilator Independent Stenosis Evaluation) study. J Am Coll Cardiol 2012;59:1392–402.

3. Härle T, Bojara W, Meyer S, Elsässer A. Comparison of instantaneous wave-free ratio (iFR) and fractional flow reserve (FFR): First real world experience. Int J Cardiol 2015;199:1–7.

4. Härle T, Meyer S, Bojara W, Vahldiek F, Elsässer A. Differences of intracoronary pressure measurement results between anterior and posterior coronary territories. Herz 2016 Aug 31 [E-pub ahead of print].

5. Toth GG, Johnson NP, Jeremias A, et al. Standardization of fractional flow reserve measurements. J Am Coll Cardiol 2016;68:742–53.

6. McCutcheon SC, Martin JL, Barnwell TO. Chapter 11: Water quality. In: Maidment DR, editor. Handbook of Hydrology. New York, NY: McGraw-Hill, 1993.

7. Hinghofer-Szalkay H. Method of high-precision microsample blood and plasma mass densitometry. J Appl Physiol (1985) 1986;60:1082–8.

8. Hinghofer-Szalkay H. Volume and density changes of biological fluids with temperature. J Appl Physiol (1985) 1985;59:1686–9.

9. Hinghofer-Szalkay H, Greenleaf JE. Continuous monitoring of blood volume changes in humans. J Appl Physiol (1985) 1987;63:1003–7.

10. Echavarria-Pinto M, Gonzalo N, Ibanez B, et al. Low coronary microcirculatory resistance associated with profound hypotension during intravenous adenosine infusion: implications for the functional assessment of coronary stenoses. Circ Cardiovasc Interv 2014;7:35–42.

11. Petraco R, Escaned J, Sen S, et al. Classification performance of instantaneous wave-free ratio (iFR) and fractional flow reserve in a clinical population of intermediate coronary stenoses: results of the ADVISE registry. EuroIntervention 2013;9:91–101.

12. De Bruyne B, Hersbach F, Pijls NH, et al. Abnormal epicardial coronary resistance in patients with diffuse atherosclerosis but "normal" coronary angiography. Circulation 2001;104:2401–6.

13. Nijjer SS, Sen S, Petraco R, et al. Pre-angioplasty instantaneous wave-free ratio pullback provides virtual intervention and predicts hemodynamic outcome for serial lesions and diffuse coronary artery disease. J Am Coll Cardiol Intv 2014;7:1386–96.

14. Kobayashi N, Maehara A, Mintz GS, et al. Usefulness of the left anterior descending artery wrapping around the left ventricular apex to predict adverse clinical outcomes in patients with anterior wall ST-segment elevation myocardial infarction (an INFUSE-AMI substudy). Am J Cardiol 2015;115:1389–95.

15. Stiermaier T, Desch S, Blazek S, Schuler G, Thiele H, Eitel I. Frequency and significance of myocardial bridging and recurrent segment of the left anterior descending coronary artery in patients with takotsubo cardiomyopathy. Am J Cardiol 2014;114:1204–9.

16. Groves SS, Jain AC, Warden BE, Gharib W, Beto RJ 2nd Severe coronary tortuosity and the relationship to significant coronary artery disease. W V Med J 2009;105:14–7.

17. Oz F, Cizgici AY, Topuz M, et al. Vitamin D insufficiency is associated with coronary artery tortuosity. Kardiol Pol 2017;75:174–80.

18. Pijls NH, van Son JA, Kirkeeide RL, De Bruyne B, Gould KL. Experimental basis of determining maximum coronary, myocardial, and collateral blood flow by pressure measurements for assessing functional stenosis severity before and after percutaneous transluminal coronary angioplasty. Circulation 1993;87:1354–67.

19. De Bruyne B, Baudhuin T, Melin JA, et al. Coronary flow reserve calculated from pressure measurements in humans: validation with positron emission tomography. Circulation 1994;89:1013–22.

20. Layland J, Wilson AM, Whitbourn RJ, et al. Impact of right atrial pressure on decision-making using fractional flow reserve (FFR) in elective percutaneous intervention. Int J Cardiol 2013;167:951–3.

21. Kostkiewicz M, Tracz W, Olszowska M, Podolec P, Drop D. Left ventricular geometry and function in patients with aortic stenosis: gender differences. Int J Cardiol 1999;71:57–61.

22. Dobson LE, Fairbairn TA, Musa TA, et al. Sex-related differences in left ventricular remodeling in severe aortic stenosis and reverse remodeling after aortic valve replacement: a cardiovascular magnetic resonance study. Am Heart J 2016;175:101–11.

23. Villari B, Campbell SE, Schneider J, Vassalli G, Chiariello M, Hess OM. Sex-dependent differences in left ventricular function and structure in chronic pressure overload. Eur Heart J 1995;16:1410–9.

24. Ng MK, Yeung AC, Fearon WF. Invasive assessment of the coronary microcirculation: superior reproducibility and less hemodynamic dependence of index of microcirculatory resistance compared with coronary flow reserve. Circulation 2006;113:2054–61.

25. Echavarria-Pinto M, van de Hoef TP, Serruys PW, Piek JJ, Escaned J. Facing the complexity of ischaemic heart disease with intracoronary pressure and flow measurements: beyond fractional flow reserve interrogation of the coronary circulation. Curr Opin Cardiol 2014;29:564–70.

KEY WORDS fractional flow reserve, FFR, iFR, instantaneous wave-free ratio